The Arecibo Legacy Fast ALFA Survey:
III. HI Source Catalog of the Northern Virgo Cluster Region

Riccardo Giovanelli[1,2], Martha P. Haynes[1,2], Brian R. Kent[1], Amélie Saintonge[1], Sabrina Stierwalt[1], Adeel Altaf[3], Thomas Balonek[4,2], Noah Brosch[5], Shea Brown[6], Barbara Catinella[7], Amy Furniss[8], Josh Goldstein[3], G. Lyle Hoffman[3], Rebecca A. Koopmann[9,2], David A. Kornreich[8] Bilal Mahmood[9] Ann M. Martin [1], Karen L. Masters [10], Arik Mitschang[8], Emmanuel Momjian[7], Prasanth H. Nair[11], Jessica L. Rosenberg[12], Brian Walsh[4]

ABSTRACT

We present the first installment of HI sources extracted from the Arecibo Legacy Fast ALFA (ALFALFA) extragalactic survey, initiated in 2005. Sources have been extracted from 3-D spectral data cubes exploiting a matched filtering technique and then examined interactively to yield global HI parameters. A total of 730 HI detections are catalogued within the solid angle $11^h44^m <$ R.A.(J2000) $< 14^h00^m$ and $+12° <$ Dec.(J2000) $< +16°$, and redshift range -1600 km s^{-1} $< cz < 18000$ km s^{-1}. In comparison, the HI Parkes All-Sky Survey (HIPASS) detected 40 HI signals in the same region. Optical counterparts are assigned via examination of digital optical imaging databases. ALFALFA HI detections are reported for three distinct classes of signals: (a) detections, typically with S/N > 6.5; (b) high velocity clouds in the Milky Way or its periphery; and (c) signals of lower S/N (to ~ 4.5) which coincide spatially with an

[1]Center for Radiophysics and Space Research, Space Sciences Building, Cornell University, Ithaca, NY 14853. *e−mail:* riccardo@astro.cornell.edu, haynes@astro.cornell.edu, bkent@astro.cornell.edu, amartin@astro.cornell.edu, amelie@astro.cornell.edu, sabrina@astro.cornell.edu

[2]National Astronomy and Ionosphere Center, Cornell University, Space Sciences Building, Ithaca, NY 14853. The National Astronomy and Ionosphere Center is operated by Cornell University under a cooperative agreement with the National Science Foundation.

[3]Hugel Science Center, Lafayette College, Easton, PA 18042. *e−mail:* hoffmang@lafayette.edu, goldstj@lafayette.edu, altafa@lafayette.edu

[4]Dept. of Physics & Astronomy, Colgate University, Hamilton, NY 13346. *e−mail:* tbalonek@mail.colgate.edu, bwalsh@bu.edu

[5]The Wise Observatory & The School of Physics and Astronomy, Raymond & Beverly Sackler Faculty of Exact Sciences, Tel Aviv University, Israel. *e−mail:* noah@wise.tau.ac.il

[6]Astronomy Dept., U. of Minnesota, 116 Church St. SE, Minneapolis, MN 55455. *e−mail:* brown@astro.umn.edu

[7]Arecibo Observatory, National Astronomy and Ionosphere Center, Arecibo, PR 00612. *e−mail:* bcatinel@naic.edu, emomjian@naic.edu

[8]Dept. of Physics, Humboldt State University, Arcata, CA 95521. *e−mail:* dak24@humboldt.edu

[9]Dept. of Physics & Astronomy, Union College, Schenectady, NY 12308. *e−mail:* koopmanr@union.edu, mahmoodb@union.edu

[10]Harvard–Smithsonian Center for Astrophysics, 60 Garden St. MS 65, Cambridge MA 02138–1516. *e−mail:* kmasters@cfa.harvard.edu

[11]Astronomy Dept., Swain West 319, Indiana University, Bloomington, IN 47405. phnair@astro.indiana.edu

[12]Harvard–Smithsonian Center for Astrophysics, 60 Garden St. MS 65, Cambridge MA 02138–1516, currently at George Mason University. *e−mail:* jrosenb4@gmu.edu

optical object of known similar redshift. Although this region of the sky has been heavily surveyed by previous targeted observations based on optical flux– or size– limited samples, 69% of the extracted sources are newly reported HI detections. The resultant positional accuracy of HI sources is dependent on S/N: it averages $24''$ ($20''$ median) for all sources with S/N > 6.5 and is of order $\sim 17''$ ($14''$ median) for signals with S/N > 12. The median redshift of the sample is ~ 7000 km s^{-1} and its distribution reflects the known local large scale structure including the Virgo cluster and the void behind it, the A1367-Coma supercluster at $cz \sim 7000$ km s^{-1} and a third more distant overdensity at $cz \sim 13000$ km s^{-1} . Distance uncertainties in and around the Virgo cluster perturb the derived HI mass distribution. Specifically, an apparent deficiency of the lowest HI mass objects can be attributed, at least in part, to the incorrect assignment of some foreground objects to the cluster distance. Several extended HI features are found in the vicinity of the Virgo cluster. A small percentage (6%) of HI detections have no identifiable optical counterpart, more than half of which are high velocity clouds in the Milky Way vicinity; the remaining 17 objects do not appear connected to or associated with any known galaxy. Based on these initial results, ALFALFA is expected to fulfill, and even exceed, its predicted performance objectives in terms of the number and quality of HI detections.

Subject headings: galaxies: spiral; — galaxies: distances and redshifts — galaxies: halos — galaxies: luminosity function, mass function — galaxies: photometry — radio lines: galaxies

1. Introduction

Because the evolution of the HI content with time promises to be a powerful tracer of galaxy evolution even into the so-called "Dark Ages", it remains imperative to understand fully the true census of HI-bearing objects at $z \sim 0$. As spectroscopic tracers, HI emission line profiles yield not only the redshift, but also measures of the total HI mass and the radial component of the rotational velocity via the HI line width, thus providing quantitative insight into the gas content and total mass. At the same time that wide area optical (e.g. Sloan Digital Sky Survey: SDSS; York *et al.* 2000) and near-infrared (e.g. Two-Micron All-Sky Survey: 2MASS; Skrutskie *et al.* 2006) surveys have been cataloging millions of galaxies, the HI Parkes All-Sky Survey (HIPASS; Barnes *et al.* 2001) produced the first wide area blind extragalactic HI line survey. HIPASS covered ~ 30000 deg^2, producing a final catalog (Meyer *et al.* 2004) of 4315 HI detections south of Dec. $= +2°$, and another 1002 (Wong *et al.* 2006) between $+2° <$ Dec $< +20°$. Because HIPASS was limited in depth and resolution, it did not sample adequate volume to yield a "cosmologically fair" sample of the universe; the median redshift of HIPASS sources is ~ 2800 km s^{-1} , near the outer boundary of the Local Supercluster. Of critical importance for the determination of the faint-end slope of the HI mass function (HIMF), only a handful of galaxies of very low HI mass were detected, and those were so near the Milky Way that distance uncertainties make their HI masses likewise highly uncertain (Masters *et al.* 2004).

HI line surveys are of special importance when combined with optical/IR surveys so that both the stellar and gaseous components are sampled. As was shown also by earlier studies such as the Arecibo Dual Beam Survey (ADBS: Rosenberg & Schneider 2002), blind HI surveys detect a population of low surface brightness, gas rich objects which are often missed by magnitude limited optical and near-IR samples. Likewise, not all galaxies exhibit detectable HI line emission, and HI surveys are limited to some degree by their positional accuracy and angular resolution since the telescopes involved have relatively large beam sizes. A true accounting of the extragalactic census must incorporate full sampling of the population of gas-rich objects sampled by HI surveys in complement to the stellar-rich ones detected by surveys like SDSS and 2MASS.

Based both on the success of HIPASS and its limitations, we have initiated a "second generation" HI blind survey, the Arecibo Legacy Fast ALFA (ALFALFA) survey, which exploits the availability of the new multi-beam Arecibo L-band Feed Array (ALFA) on the 305 m antenna. ALFALFA will require ~ 4000 hours of telescope time to survey ~ 7000 deg^2 of the high galactic latitude sky visible from Arecibo (Giovanelli *et al.* 2005a: Paper I). HIPASS used a 13 beam receiver on the Parkes 62-m telescope (15.5′ HPBW); ALFALFA exploits a similar 7-feed receiver array on the 305-m Arecibo telescope ($\sim 3.5′$). The survey design of ALFALFA exploits the superior collecting area and angular resolution of the Arecibo telescope as well as the broader bandwidth and spectral resolution of its digital correlator. Furthermore, ALFALFA makes use of automated signal detection techniques to produce source catalogs unbiased by the width of the HI signal (Saintonge 2007). Designed to surpass significantly the HI survey benchmark established by HIPASS, ALFALFA improves on its predecessor by a factor of ~ 8 in sensitivity, ~ 4 in angular resolution, ~ 3 in spectral resolution and ~ 1.6 in spectral coverage. The added depth of ALFALFA will allow it to sample a "fair" volume of the Universe. In particular, ALFALFA will sample well the volume corresponding to the so-called "convergence depth" (Giovanelli *et al.* 1998; Dale & Giovanelli 2000) which contributes most of the peculiar velocity of the Milky Way with respect to the Cosmic Microwave Background.

Simulations presented in Paper I predicted that ALFALFA will detect some 20,000 extragalactic HI line sources, from very nearby low mass dwarfs to massive spirals at $z \sim 0.06$. The survey is designed specifically to determine robustly the HIMF in the local universe and will at the same time provide a census of HI in the surveyed sky area, making it especially useful in synergy with other wide area surveys such as SDSS, 2MASS, GALEX, ASTRO–F, etc. The full scope and goals of the survey are described further in Paper I.

HI line surveys yield three principal observational parameters: the integrated HI line flux, the systemic redshift and the Doppler line width. For resolved objects, they can also yield an estimate of the HI size, and if the source fills the beam, the HI column density. ALFALFA is expected to resolve about 500 nearby galaxies; other objects with exceptionally extended HI distributions will also be mapped. Its positional accuracy (see Section 5) allows identification of the optical counterparts of the HI detections by immediate cross reference with the large optical/IR imaging databases. The most interesting objects will perhaps be the isolated HI sources which may *not* have optical counterparts, the so-called "dark galaxies".

The ALFALFA survey was initiated in February 2005. Since then, we have conducted observations regularly and anticipate allocations of 700–900 hours of telescope time per year. In order to provide timely information to the community, a public web site *http://egg.astro.cornell.edu/alfalfa* is updated regularly to provide survey plans and status information. Because of the 2-pass drift mode observing strategy (Paper I), complete spectral coverage combines many separate datasets obtained over observing periods spread over many months. Final 3-D cubes from which signals can be reliably extracted cannot be produced until the entire dataset covering a targeted region is acquired. In fact, the first-year datasets were rather incomplete, so that construction of full-coverage 3-D data cubes has been possible only recently.

Given the area of sky visible to the Arecibo telescope, a prime target for ALFALFA is the Virgo cluster and its surroundings. Although the spirals in the core of the Virgo cluster are strongly HI deficient (Davies & Lewis 1973; Chamaraux *et al.* 1980; Giovanelli & Haynes 1983; Solanes *et al.* 2002), the cluster periphery contains many known optical late-type galaxies. ALFALFA is specifically designed to detect objects of relatively low HI mass, $\sim 3 \times 10^7 M_\odot$, at the Virgo distance. Hence, the Virgo region of the sky was targeted by ALFALFA from the beginning; its central region has been the first zone to be surveyed completely. In this paper, we present a catalog of HI sources extracted from two constant declination strips of 3-D grids, covering a swath $4°$ wide in Declination $+12° < \text{Dec.(J2000)} < +16°$ and stretching $33°$ in Right Ascension between $11^h44^m < \text{R.A.(J2000)} < 14^h00^m$. This area includes the northern section of the Virgo cluster.

With a complete dataset now in hand for a first installment covering 132 deg^2, this paper presents the first ALFALFA HI detection catalog, in the spirit of prompt access which the legacy nature of the survey promises. A catalog containing sources of the southern part of the Virgo cluster region is in preparation (Kent *et al.* 2007).

In Section 2 we discuss the ALFALFA survey observations and data analysis. In Section 3, we briefly discuss issues related to the data quality of the region sampled by the catalog, as well as signal extraction criteria. The contents of the catalog are also described. Section 4 gives an overview of the statistical properties of the cataloged sample. The positional accuracy of the HI positions is discussed in Section 5. Section 6 summarizes the HI detections presented here and what the results of this first installment predict for the future results of the full ALFALFA survey. A Hubble constant of 70 km s^{-1} Mpc^{-1} is used for distance dependent calculations, unless otherwise specified.

2. Observations and Data Reduction

ALFALFA uses the 7–feed ALFA receiver system and a spectral line backend capable of instantaneously producing spectra from the two linear polarizations of each beam and covering a bandwidth of 100 MHz. The angular resolution of the survey is given by the elliptical shape of each of ALFA's beams, $3.3' \times 3.8'$ (Paper I), and the spectral resolution is 25 kHz, which translates to about 5.5 km s^{-1} at $cz \sim 0$ km s^{-1} before spectral smoothing is applied. ALFALFA surveys the sky with the telescope in "almost fixed azimuth" drift mode: the telescope azimuth arm is placed on the meridian, and the sky drifts by. Small adjustments of the zenith angle are applied throughout the observing period to maintain the beam tracks at constant J2000 Dec. Each region of sky is visited twice, at two epochs spaced by a few months in the Earth's orbit about the Sun. No Doppler tracking of the Local Oscillator frequency is employed, so that cosmic signals shift in frequency between the two epochs by the difference in their heliocentric velocities, projected along the line of sight. The resulting coverage yields parallel tracks of constant J2000 Dec., separated from one another by $1.05'$. The sampling rate in R.A. is 1 Hz. In both coordinates, the sampling is significantly better than the Nyquist rate. Data-taking for ALFALFA was initiated in February 2005 and, in the practical context of time allocation at a widely used, multidisciplinary national facility like Arecibo, completion of the full survey is projected to require about 6 years. More technical detail regarding the equipment, observing mode and sensitivity issues can be found in Paper I.

The ALFALFA data processing scheme has been briefly outlined in Paper I and will be described in detail elsewhere (Giovanelli *et al.* 2007, in preparation; Saintonge 2007, submitted). Full processing of all survey data to level I — which includes bandpass calibration, radio frequency interference (hereafter "rfi") flagging, continuum source identification and extraction of drift scans — is carried out shortly after data taking, as anticipated in Paper I. However, the production of 3-D data cubes which fully sample a region of sky requires the completion of both passes and thus cannot be completed until all data covering that region are in hand. In Paper I, we discussed the parceling of the sky in data processing units we referred to as "tiles", of 10^m in R.A. by $4°$ in Dec. In practice, as the processing needs demanded a distributed strategy, data units of smaller size than the above mentioned tiles were found to be compatible with a "minimum denominator" computer performance. The data units thus adopted each cover a sky area of $2.4° \times 2.4°$ in R.A. and Dec.; in order to avoid confusion with the previous definition of tiles, we refer to regularly gridded data cubes of $2.4° \times 2.4°$ and preset centers as "grids". Centers of grids that are adjacent in R.A. are separated from each other by 8^m; the separation in Dec. is $2°$. A spatial overlap of about 20% in each coordinate allows effective spatial coverage of all sources found in the overlap regions. In order to maintain the gridded data

file size at a limit comfortably manipulated by modest computer hardware, we break each spatial grid into four overlapping spectral subgrids of 1024 channels each, after discarding the bandends. Because of rfi, the spectral resolution is not reduced at this stage, and, the full information on spectral weights, as described in Sectin 2.3 below, is retained. Each 1024 channel 3-D spectral cube has a final size of 380 MB.

2.1. Access to Data Products

In the interest of timely access to our data products by the community, we plan to release source catalogs at the earliest possible time, consistent with the legacy character of ALFALFA. The catalog presented here is the first part of an archival database being developed as a collaborative project with the National Astronomy and Ionosphere Center and the Cornell Theory Center. The data catalog products will be available at *http://arecibo.tc.cornell.edu/hiarchive*[13] as a node of the U.S. National Virtual Observatory (NVO). Included already at that website are catalogs and spectral data products of targeted single-beam HI observations of ~9000 galaxies observed by our group (Springob *et al.* 2006) and the ALFALFA precursor observations (Paper II). At the time of publication of this paper, the catalog presented here and access to the spectral profiles associated with the HI detections will be incorporated into our existing HI digital archive. An ongoing development effort aims its focus on the protocol for long–term public delivery of the 3–D ALFALFA data set through web–based access tools. At this time, delivery of the 3-D data is made possible through the observing team itself, by direct contact to R.G. or M.P.H.. A major challenge is data volume: each of the 3-D cubes covering the 34 individual "grids" constituting the current catalog require 1.5 GB. Allowing access and manipulation of the gridded data publicly will require the development of distributed computational tools.

In this work, we present a catalog of HI sources extracted from the ALFALFA grids covering a region stretching from $+12°$ to $16°$ in Dec. and from 11^h44^m to 14^h00^m in R.A. For reference to our database, the denominations of the grids constituting this catalog are 1148+13 to 1356+13 and 1148+15 to 1356+15, in steps of 8^m in R.A. The solid angle subtended by this region is ~132 deg^2, which is ~ 1.9% of the sky to be ultimately surveyed by ALFALFA. The coverage of the region is complete by the target goals of ALFALFA, i.e. the region has been sampled by two separate passes with the ALFA array in drift mode. The average quality of the data is fair to excellent; details on the data quality at a particular location can be garnered by consultation with any of the Cornell authors or by consultation of the ALFALFA website mentioned in Section 1. This type of information will eventually be accessible through our NVO–compliant node.

2.2. Impact of M87

The surveyed region includes the northern part of the Virgo cluster and M87, at $RA = +12^h30^m49.4^s$, $Dec = 12°23'28''$. The very strong radio source associated with M87 has a 1.4 GHz continuum flux of 220 Jy, which increases the system temperature of the Arecibo telescope at L band by a factor of 70 when M87 crosses within the main beam of the telescope. Even when M87 is detected only through the near sidelobe structure of the beam, the sensitivity decreases drastically both because of the increased system temperature and because of the onset of strong spectral standing waves. Effectively, a region of about $1°$ to $1.5°$ radius

---

[13]This research has made use of data obtained from or software provided by the US National Virtual Observatory, which is sponsored by the National Science Foundation.

centered on M87 remains inaccessible to HI spectroscopy except for the very brightest HI sources, as we illustrate in Section 4.
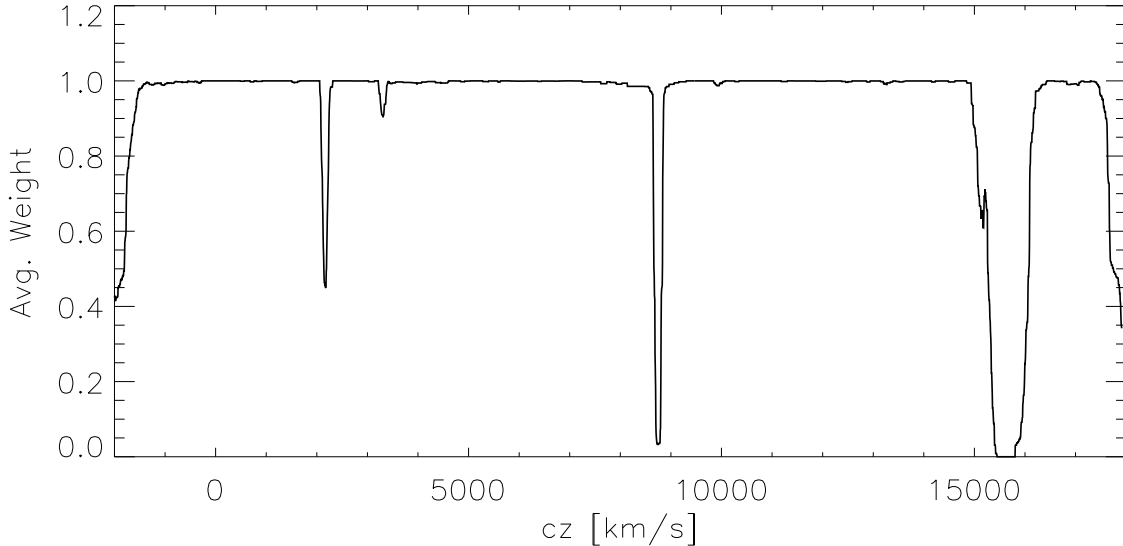

Fig. 1.— Average spectral weights for the region of this catalog, plotted vs. heliocentric recessional velocity. The steep dropoff at each end of the spectral domain is an instrumental effect associated with the spectrometer bandpass edge. The other strong troughs are associated with rfi originating with the San Juan FAA radar operating at 1350 MHz.

2.3. Radio Frequency Interference

In practice, rfi contaminates certain regions of the observed spectral window. The data processing pipeline tracks the flagging from visual inspection of spectral samples which are deemed to be contaminated and assigns a weight to each pixel in 3-D space according to the degree of this flagging. The quality of the spectral coverage is exemplified in Figure 1, which shows the average "spectral weight" over the full region sampled by the present source catalog. A spectral weight of 1.0 indicates good data quality and full utilization of all the data at that frequency or cosmological recession velocity. We compute an array of spectral weights, which is a quality estimator, for each spatial pixel of the survey. The drops in the spectral weights at both ends of the graph in Figure 1 arise from the diminished sensitivity found at the bandpass edges resulting from instrumental effects. The deep trough between 15000 and 16000 km s^{-1} is due to rfi originating from the Federal Aviation Administration radar operating at 1350 MHz near the Luiz Muñoz Marin airport in San Juan. The narrower features at 8800 km s^{-1}, 3300 km s^{-1} and 2200 km s^{-1} are modulations of the 1350 MHz radar signal occurring within the spectrometer. While the feature between 15000 and 16000 km s^{-1} renders inaccessible a larger cosmic volume, the feature at 8800 km s^{-1} affects a larger number of possible detections, given its spectral location in vicinity of the peak of the redshift distribution for our catalog. On average, about 85% of the spectral bandpass is clear for astronomical use.

The presence of rfi causes distinct volumes of the universe, which correspond to the frequency ranges of

redshifted HI, to be "obscured" to ALFALFA. In order to maintain a proper census of the survey volume, we use the 3-D "pixel mask" which records the spectral weights described above.

3. Source Catalog

Shortly after each observing session, the individual 600-sec drift scans are processed to Level I, that is, they are bandpass subtracted and calibrated, and flagging of channels affected by rfi is performed (see Paper I). Once a region of the sky has been fully sampled by ALFALFA, a 3-D grid is then generated from all of the individual drift scans that cross it. In practice, the band edges are dropped, and four spectral subgrids, each comprising 1024 channels, with ~ 100 channel overlap of each, are constructed for each $2.4° \times 2.4°$ spatial grid. Each spectral subgrid is then "flat fielded" (i.e. baselined) and made ready for source extraction. An automatic signal extractor described in Saintonge (2007) that operates in the Fourier domain produces a preliminary catalog of sources to a specified threshold in signal-to–noise ratio (hereafter S/N). Each candidate source is then examined visually and a decision on its inclusion in a final catalog, as well as a detailed, interactively obtained set of measurements yielding the principal source parameters, is made. A spatially integrated spectrum of the source and a postage–stamp 3D section of the grid centered on the source are archived.

After HI source candidates are inspected, measured and cataloged, identification of possible optical counterparts is carried out through inspection of the Sloan Digital Sky Survey (hereafter SDSS) [14], DSS2 via *Skyview*[15], NED[16] and our privately maintained data base of extragalactic sources (the "AGC", for "Arecibo General Catalog"). For the vast majority of HI source candidates of fair to excellent S/N, a relatively unambiguous identification of an optical counterpart is possible, thanks to the positional accuracy of the HI sources, as described in Section 5. In our catalog we distinguish between 3 kinds of sources: (a) reliable, extragalactic HI candidate sources, down to a S/N threshold of approximately S/N=6.5 (the limit is soft, as described further below); (b) high S/N features of low velocity likely to be galactic or peri–galactic High Velocity Clouds (HVCs); (c) candidate HI sources of lower S/N (approximately 4.5 to 6.5), corroborated by the vicinity of a possible optical counterpart of the same redshift. The signal extraction process also yields candidate sources of lower S/N than those listed in the present catalog. A list of those objects is available upon request. As discussed in Paper I, the most efficient strategy for confirming follow-up observations requires a high sky density of sources spread in cz but at similar declination. Possible detections of low S/N will be observed in follow-up corroborating runs, which will help us quantify the reliability, i.e. the fraction of candidate sources which observations will confirm as real, as a function of the measured S/N. Those

---

[14]Funding for the Sloan Digital Sky Survey (SDSS) has been provided by the Alfred P. Sloan Foundation, the Participating Institutions, the National Aeronautics and Space Administration, the National Science Foundation, the U.S. Department of Energy, the Japanese Monbukagakusho, and the Max Planck Society. The SDSS Web site is http://www.sdss.org/. The SDSS is managed by the Astrophysical Research Consortium (ARC) for the Participating Institutions. The Participating Institutions are The University of Chicago, Fermilab, the Institute for Advanced Study, the Japan Participation Group, The Johns Hopkins University, Los Alamos National Laboratory, the Max-Planck-Institute for Astronomy (MPIA), the Max-Planck-Institute for Astrophysics (MPA), New Mexico State University, University of Pittsburgh, Princeton University, the United States Naval Observatory, and the University of Washington.

[15]*Skyview* was developed and maintained under NASA ADP Grant NAS5–32068 under the auspices of the High Energy Astrophysics Science Archive Research Center at the Goddard Space Flight Center Laboratory of NASA.

[16]The NASA/IPAC Extragalactic Database (NED) is operated by the Jet Propulsion Laboratory, California Institute of Technology, under contract with the National Aeronautics and Space Administration.

observations will also deliver a significant addition of reliable detections, at a very low "cost" of telescope time per source (see Papers I and II).

A few details should be kept in mind in the use of the contents of Table 1, as described below:

- Several objects straddle or are confused by the HI emission from the Milky Way. A spectrum of the object is generally obtained by subtracting a median spectrum obtained over a square perimetral segment of pixels around the source, from the inner part of the perimeter populated by the source. In some cases, interpolation of the spectrum across the Milky Way emission provides an adequate result. Sources for which these intrusive techniques are applied are noted in the footnotes to Table 1.

- Sources are often detected in the spectral vicinity of rfi features. Interpolation across the region affected by rfi is often necessary. While the detection of the source may be clear, accurate measurement of its parameters may be impossible and much caution should be adopted in their use. This problem is frequent for sources between $cz \sim 8500$ km s^{-1} and $cz \sim 8900$ km s^{-1} , a spectral region not far removed from the median redshift of our catalog. Each of these cases is noted in the footnotes to Table 1.

- Extended sources containing multiple concentrations, obviously physically associated, are sometimes found. We adopt the practice of measuring separately each of the concentrations and report them in Table 1 as separate entries. They are also noted in the footnotes to Table 1.

Table 1 contains the principal parameters of HI candidate detections, namely:

Col. 1: an entry number for this catalog.

Col. 2: the source number in the Arecibo General Catalog, a private database of extragalactic objects maintained by M.P.H. and R.G. The AGC entry normally corresponds to the optical counterpart except in the cases of HI sources which cannot be associated with an optical object with any high degree of probability.

Col. 3: center (J2000) of the HI source, after correction for systematic telescope pointing errors, which range between a few and about a dozen arcsec, as described in Section 5. The accuracy of the HI positions depends on source strength. On average, the positional accuracy is about $24''$. See Section 5 for details.

Col. 4: center (J2000) of the optical galaxy found to provide a reasonable optical counterpart. This position has been checked for each listed object and assessed using tools provided through the SDSS and *Skyview* websites. Quality of centroids is estimated to be $2''$ or better. The assessment of identification between optical and HI sources is based on spatial proximity, redshift (if optical is available), morphology, color and evidence for optical emission lines (if known). For sources with no discernible optical counterpart and those for which such assignment is ambiguous, due to the presence of more than one equally possible optical counterpart, no optical position is listed. The latter set includes HVCs. For objects with more than one possible candidate as an optical counterpart but such that one of the candidates is significantly more preferable than the others, an optical identification is made; however, a comment on the possible ambiguity is added in the notes to this table, as alerted by an asterisk in Col. 12.

Col. 5: heliocentric velocity of the HI source, $cz_\odot$, measured as the midpoint between the channels at which the flux density drops to 50% of each of the two peaks (or of one, if only one is present) at each side of the spectral feature. Units are km s^{-1} . The error on $cz_\odot$ to be adopted is half the error on the width, tabulated in Col. 6.

Col. 6: velocity width of the source line profile, $W50$, measured at the 50% level of each of the two peaks, as described for Col. 5. This value is corrected for instrumental broadening. No corrections due to turbulent motions, disk inclination or cosmological effects are applied. Between brackets we show the estimated error on the velocity width, ϵ_w, in km s^{-1} . This error is the sum in quadrature of two components: the first is a statistical error, principally dependent on the S/N ratio of the feature measured; the second is a systematic error associated with the subjective guess with which the observer estimates the spectral boundaries of the feature: maximum and minimum guesses of the spectral extent of the feature are flagged and the ratio of those values is used to estimate systematic errors on the width, the velocity and the flux integral. In the majority of cases, the systematic error is significantly smaller than the statistical error; thus the former is ignored.

Col. 7: integrated flux density of the source, F_c, in Jy km s^{-1} . This is measured on the integrated spectrum, obtained by spatially integrating the source image over a solid angle of at least $7' \times 7'$ and dividing by the sum of the survey beam values over the same set of image pixels (see Shostak & Allen 1980). Estimates of integrated fluxes for very extended sources with significant angular asymmetries can be misestimated by our algorithm, which is optimized for measuring sources comparable with or smaller than the survey beam. A special catalog with parameters of extended sources will be produced after completion of the survey. The estimated uncertainty of the integrated flux density, in Jy km s^{-1} is given between brackets. Uncertainties associated with the quality of the baseline fitting are not included; an analysis of that contribution to the error will be presented elsewhere for the full survey. See description of Col. 6 for the contribution of a possible systematic measurement error.

Col. 8: signal–to–noise ratio S/N of the detection, estimated as

$$S/N = \left(\frac{1000F_c}{W50}\right)\frac{w_{smo}^{1/2}}{\sigma_{rms}} \tag{1}$$

where F_c is the integrated flux density in Jy km s^{-1} , as listed in col. 7, the ratio $1000F_c/W50$ is the mean flux across the feature in mJy, w_{smo} is either $W50/(2 \times 10)$ for $W50 < 400$ km s^{-1} or $400/(2 \times 10) = 20$ for $W50 \geq 400$ km s^{-1} [w_{smo} is a smoothing width expressed as the number of spectral resolution bins of 10 km s^{-1} bridging half of the signal width], and σ_{rms} is the r.m.s noise figure across the spectrum measured in mJy at 10 km s^{-1} resolution, as tabulated in Col. 9. In a similar analysis, in Giovanelli *et al.* 2005b (hereafter Paper II) we adopted a maximum smoothing width $W50/20 = 10$. See Figure 5 and related text below for details. The value of the smoothing width could be interpreted as an indication of the degree to which spectral smoothing aids in the visual detection of broad signals, against broad–band spectral instabilities. The ALFALFA data quality appears to warrant a more optimistic adoption of the smoothing width than previously anticipated.

Col. 9: noise figure of the spatially integrated spectral profile, σ_{rms}, in mJy. The noise figure as tabulated is the r.m.s. and measured over the signal– and rfi–free portions of the spectrum, after Hanning smoothing to a spectral resolution of 10 km s^{-1} .

Col. 10: adopted distance in Mpc, D_{Mpc}. For objects with $cz_{cmb} > 3000$, the distance is simply $cz_{cmb}/H_\circ$; cz_{cmb} is the recession velocity measured in the Cosmic Microwave Background reference frame and $H_\circ$ is the Hubble constant, for which we use a value of 70 km s^{-1} Mpc^{-1}. For objects of lower cz_{cmb}, we use a peculiar velocity model for the local Universe, as described in Paper II. Objects which are thought to be parts of clusters or groups are assigned the cz_{cmb} of the cluster or group. Cluster and group membership are assigned following the method described in Springob *et al.* 2006. A detailed analysis of group and cluster membership of ALFALFA objects will be presented elsewhere. Note that the Virgo cluster extends

over much of the solid angle surveyed. This introduces unavoidable ambiguities in the distance assignment, as the peculiar flow model only corrects for large–scale perturbations in the velocity field and is unable to deal effectively with regions in the immediate vicinity of the cluster and along a section of a cone which contains the cluster, up to $cz \sim 2500$ km s^{-1} . The distance to the Virgo cluster was assumed to be 16.7 Mpc.

Col. 11: logarithm in base 10 of the HI mass, in solar units. That parameter is obtained by using the expression $M_{HI} = 2.356 \times 10^5 D_{Mpc}^2 F_c$.

Col. 12: object code, defined as follows:

Code 1 refers to sources of S/N and general qualities that make it a reliable detection. By "general qualities" we mean that, in addition to an approximate S/N threshold of 6.5, the signal should exhibit a good match between the two independent polarizations and a spatial extent consistent with expectations given the telescope beam characteristics. Thus, some candidate detections with $S/N > 6.5$ have been excluded on grounds of polarization mismatch, spectral vicinity to rfi features or peculiar spatial properties. Likewise, some features of $S/N < 6.5$ are included as reliable detections, due to optimal overall characteristics of the feature. The S/N threshold for acceptance of a reliable detection candidate is thus soft. In a preliminary fashion, we estimate that detection candidates with $S/N > 6.5$ in Table 1 are reliable, i.e. they will be confirmed in follow–up observations in better than 95% of cases (Saintonge 2007). Follow-up observations planned for 2007 will set this estimate on stronger statistical grounds.

Code 2 refers to sources of low S/N (< 6.5), which would ordinarily not be considered reliable detections by the criteria set for code 1. However, those HI candidate sources are matched with optical counterparts with known optical redshifts which match those measured in the HI line. These candidate sources, albeit "detected" by our signal finding algorithm, are accepted as likely counterparts only because of the existence of previously available, corroborating optical spectroscopy. We refer to these sources as "priors". We include them in our catalog because they are very likely to be real.

Code 9 refers to objects assumed to be HVCs; no estimate of their distances is made.

Notes flag. An asterisk in this column indicates a comment is included for this source in the text below.

Only the first few entries of Table 1 are listed in the printed version of this paper. The full contents of Table 1 are accessible through the electronic version of the paper and will be made available also through our public digital archive site.

Notes associated with the objects listed in Table 1 follow:

1-2: extended HVC?

1-20: also possible opt id with companion at 114802.6+145228

1-21: blend w/210799, params. very uncertain

1-22: blend w/212846, params. very uncertain

1-23: emission of 210799 also in spectrum

1-28: optical identification uncertain 114904.4+133746; also possible 114858.8+133710, nearer to HI but ∼1 mag fainter

1-36: possible blend; alternative optical identification is 115012.8+154620, opt z=0.045, which is 1 mag brighter, but twice as far from HI center

1-42: extended HI, blended with emission to NE

Table 1.   HI Candidate Detections

Cat. nr	AGC	HI Coords (J2000)	Opt. Coords. (J2000)	$cz_\odot$ km s^{-1}	$w50$ (ϵ_w) km s^{-1}	F_c (ϵ_f) Jy km s^{-1}	S/N	rms mJy	Dist Mpc	$\log M_{HI}$ $M_\odot$	Code
1- 1	210692	114419.8+150620	114420.2+150616	10489	283(13)	1.42(0.08)	8.6	1.85	151.5	9.89	1
1- 2	215418	114421.4+150459		247	33(2)	0.38(0.04)	6.8	2.09			9 *
1- 3	213528	114432.1+131527	114432.0+131511	10291	119(12)	0.52(0.06)	4.8	2.09	148.6	9.43	2
1- 4	213473	114437.1+124657	114439.5+124726	12751	245(88)	1.06(0.09)	5.8	2.14	183.7	9.93	2
1- 5	212928	114440.6+144551	114440.9+144555	10240	379(4)	2.32(0.08)	14.0	1.73	147.9	10.08	1
1- 6	215197	114442.2+150215	114444.0+150140	3354	103(40)	0.72(0.05)	7.1	1.78	50.4	8.63	1
1- 7	215148	114443.7+121708	114442.6+121802	10258	303(76)	1.20(0.09)	6.5	2.11	148.1	9.79	1
1- 8	210746	114524.6+142242	114522.1+142200	3342	129(25)	0.90(0.05)	10.8	1.56	50.3	8.73	1
1- 9	210753	114533.5+121240	114534.9+121218	9298	92(3)	1.40(0.06)	14.4	2.05	134.5	9.78	1
1- 10	215149	114554.6+134955	114556.1+135021	3267	38(9)	0.57(0.04)	7.6	1.77	49.2	8.51	1
1- 11	211216	114609.2+125231	114609.0+125246	3296	145(6)	1.45(0.05)	15.9	1.58	49.6	8.92	1
1- 12	6747	114622.9+134937	114624.1+134938	2696	95(4)	6.14(0.06)	58.7	1.82	41.2	9.39	1
1- 13	6753	114646.5+143208	114646.2+143158	3149	169(6)	2.10(0.06)	18.2	1.73	47.5	9.05	1
1- 14	210779	114700.3+135223	114659.7+135225	3165	231(1)	1.97(0.06)	15.9	1.63	47.2	9.01	1
1- 15	6758	114706.2+134238	114706.3+134223	3103	178(2)	7.15(0.06)	67.2	1.63	47.2	9.57	1
1- 16	215618	114720.4+152015	114716.8+151924	6401	162(12)	0.57(0.07)	4.6	2.18	93.4	9.07	2
1- 17	213478	114725.7+121308	114725.4+121239	6111	212(48)	0.64(0.08)	4.5	2.18	89.3	9.08	2
1- 18	215151	114750.3+134144	114750.7+134215	3456	72(4)	0.61(0.05)	7.3	1.79	51.9	8.59	1
1- 19	213479	114800.7+120714	114800.2+120649	9218	102(8)	0.85(0.06)	7.2	2.16	133.3	9.55	1
1- 20	215198	114801.1+145126	114800.4+145221	11840	336(23)	1.29(0.07)	6.8	1.51	170.8	9.95	1 *
1- 21	210798	114809.0+125445	114808.8+125453	6216	226(1)	3.37(0.06)	25.5	1.68	90.8	9.82	1
1- 22	6775	114812.6+131252	114812.7+131230	3165	193(0)	7.89(0.07)	59.1	1.99	47.1	9.62	1
1- 23	212846	114816.9+124330	114817.9+124333	3955	191(19)	3.82(0.08)	31.1	1.98	58.9	9.49	1 *
1- 24	210799	114821.6+124321	114820.1+124300	3969	273(17)	4.51(0.09)	24.1	1.99	59.1	9.57	1 *
1- 25	210804	114830.6+124401	114830.7+124347	3629	157(10)	1.72(0.08)	12.3	2.03	54.3	9.08	1 *
1- 26	210807	114843.8+140323	114844.0+140310	3206	224(8)	1.53(0.07)	10.9	1.85	47.2	8.90	1
1- 27	210809	114858.1+155322	114856.0+155325	17096	399(4)	1.88(0.10)	69.7	2.03	245.8	10.43	1
1- 28	215154	114901.2+133708	114904.4+133746	2981	33(10)	0.51(0.03)	8.7	1.47	45.1	8.39	1 *
1- 29	215156	114901.9+134038	114903.1+134052	7136	205(27)	1.04(0.06)	8.8	1.71	103.8	9.42	1
1- 30	213484	114908.0+123721	114912.2+123754	4054	206(35)	0.73(0.08)	4.7	2.16	60.3	8.80	2
1- 31	215200	114913.0+153708	114914.1+153651	16951	376(29)	2.13(0.11)	10.1	2.31	243.7	10.47	1
1- 32	210814	114920.7+152426	114920.1+152432	6371	163(2)	1.66(0.07)	12.2	2.27	93.0	9.53	1
1- 33	215158	114942.0+122404	114940.1+122338	3201	129(4)	0.73(0.05)	8.0	1.70	48.2	8.60	1
1- 34	210820	114943.4+131455	114941.4+131441	6141	207(2)	1.29(0.07)	9.8	1.82	89.7	9.39	1
1- 35	210822	115002.6+150132	115002.7+150124	756	45(3)	1.49(0.04)	18.2	1.70	8.6	7.42	1
1- 36	215229	115007.5+154613	115008.0+154702	13303	338(86)	1.76(0.10)	9.6	2.09	191.7	10.18	1 *
1- 37	215202	115011.4+143926	115009.7+143918	6485	192(4)	1.39(0.08)	9.7	2.08	94.6	9.47	1
1- 38	213488	115018.9+124333	115016.4+124327	7774	203(5)	0.88(0.08)	5.5	2.28	112.8	9.42	2
1- 39	215203	115038.1+142719	115037.8+142712	6082	76(3)	0.72(0.04)	9.1	1.63	88.9	9.13	1
1- 40	215204	115045.4+144538	115044.8+144633	16443	311(38)	1.07(0.08)	5.5	1.88	236.5	10.15	2

1-44: no identifiable optical counterpart: appendage of 215231?

1-46: HI emission merges in spectral region w/strong rfi; HI parms. very uncertain

1-62: no clear opt counterpart; UGC 6911 5.3′ to W, similar cz; HI feature appears real, not sidelobe effect

1-70: HI emission on edge of bandpass, poor sensitivity, params uncertain

1-98: very near edge of bandpass: poor sensitivity, params uncertain

1-109: alternative opt id: 120521.3+153110, a much fainter obj but nearer to HI position

1-113: 120625.3+132303 is in a pair with 120626.0+132254; HI emission could be associated with either or both

1-116: no opt counterpart, extended HI: compact HVC (cHVC)?

1-122: no opt counterpart, extended HI: HVC

1-124: HI emission on edge of bandpass, poor sensitivity, parms uncertain

1-129: HI merges in spectral region affected by rfi; parms of detection very uncertain

1-130: no optical counterpart; extended HI: HVC projected in vicinity of NGC 4192

1-148: no optical counterpart; extended HI: HVC projected in vicinity of NGC 4192

1-153: no optical counterpart; extended HI: HVC projected in vicinity of NGC 4192

1-157: no optical counterpart; extended HI: HVC projected in vicinity of NGC 4192

1-158: HI emission may have SW to NE extension

1-162: no optical counterpart; extended HI: HVC projected in vicinity of NGC 4192

1-173: no identifiable optical counterpart

1-184: no identifiable optical counterpart; extended HI: HVC projected in vicinity of NGC 4192

1-185: no identifiable optical counterpart

1-210: no optical counterpart, S of U7284" galaxy appendage or HVC?

1-214: HI pos matches that of IC 3080, which has discordant opt z; match with 121607.0+141237 based on similarity of z, but note large pos discrepancy: ambiguous opt identification

1-217: no identifiable optical counterpart; extended HI: HVC projected in vicinity of NGC 4192

1-228: no identifiable optical counterpart; extended HI: HVC projected in vicinity of NGC 4192

1-229: alternative optical identification is 121716.7+142732, opt brighter but farther from HI center

1-235: no identifiable optical counterpart; portion of Virgo HI21 (Davies *et al.* 2004; Minchin *et al.* 2005)

1-238: no identifiable optical counterpart; portion of Virgo HI21 (Davies *et al.* 2004; Minchin *et al.* 2005)

1-239: no identifiable optical counterpart; portion of Virgo HI21 (Davies *et al.* 2004; Minchin *et al.* 2005)

1-241: in vicinity of Virgo HI21 (Davies *et al.* 2004; Minchin *et al.* 2005)

1-242: no identifiable optical counterpart; unresolved, compact HVC projected in vicinity of NGC 4192

1-245: no identifiable optical counterpart; unresolved, compact HVC projected in vicinity of NGC 4192

1-257: no identifiable optical counterpart; 4′ N of HI121910.9+125322=A220351: tidal appendage?

1-260: resolved disk, elongated SW (hi vel) to NE (lo vel); previous HI cz=1280 appears to be wrong

1-263: crowded opt field, ambiguous opt id; alternative opt counterparts are 121942.5+132549, 121948.4+132522, 121945.1+132627

1-264: no identifiable optical counterpart; barely resolved, compact HVC

1-271: no identifiable optical counterpart; VCC429 at 122043.8+143751 and similar z is at 2.3′ to NE; HI assumed related.

1-276: blend of U7412 and U7418 (N4298 and N 4302); HI flux mainly of U7418

1-278: opt counterpart is close galaxy pair

1-279: no identifiable optical counterpart; unresolved, compact HVC

1-287: v uncertain separation from MW HI; marginal detection and v poor HI parms

1-309: uncertain separation from MW HI

1-312: v poor positional match, marginal S/N, id

1-316: 3.6′ to SE of M86=U7532, no identifiable opt counterpart; part of Virgo HI4 (Davies *et al.* 2004; note that the declination listed in that paper is incorrect) and shown to be a plume extending from NGC 4388, by Oosterloo & van Gorkom (2005)

1-318: uncertain separation from MW HI

1-336: extended HI source, blend of 123115.0+141148 and 123120.0+131144; id assignment of HI to 123115.0+141148 on vicinity grounds

1-347: fainter opt galaxy at 123355.2+135554 also possible counterpart

1-352: no clearly identifiable opt counterpart

1-354: no identifiable opt counterpart; in spite of fair S/N, doubts on reality, due to standing waves produced by vicinity to M87

1-359: opt counterpart is extremely lsb, v extended object? however, vicinity of M87 makes HI detection somewhat doubtful

1-360: no identifiable opt counterpart, marginal S/N

1-366: no identifiable opt counterpart

1-371: ambiguous opt id: 123650.8+141506 possible; 224865, identified with 123643.1+141611, 2.7′ to NW, is at similar z (NGC 4571 in foreground)

1-377: optical id ambiguous: other possibilities are 123857.5+142435 and 123859.1+142457

1-386: on edge of band, ragged data

1-391: blend with 7874=N4633, interact syst, and interference with MW HI; parms uncertain

1-392: most of emission in profile is associated with source U7874, identified with U7884=N4639, 2.8′ E; feature measured is wing to high velocity side of emission peak

1-397: extended emission of U7902=N4654 overwhelms the field; emission tentatively assigned to opt galaxy at 124412.0+125631 is low velocity wing of line

1-398: positional offset of 1′ between opt and HI probably real, not centroiding error

1-399: optical identification with very faint lsb feature, 3.5′ to SE of IC3720

1-402: ambiguous opt id: also possible 124514.7+141906

1-409: on edge of band, ragged data

1-417: optical identification with faint blue obj is very tentative

1-426: other possible opt counterpart at 125209.6+150456, marginally farther away

1-451: alternative opt id: fainter obj at 125911.0+142519

1-474: optical identification with bluest galaxy in triplet

1-488: on edge of band, ragged data

1-493: on edge of band, ragged data

1-494: no identifiable opt counterpart, extended HI: part of HVC complex

1-497: no identifiable opt counterpart, extended HI: part of HVC complex

1-500: no identifiable opt counterpart, extended HI: part of HVC complex

1-502: no identifiable opt counterpart, extended HI: part of HVC complex

1-504: gal emission merges in region affected by rfi: parms uncertain

1-507: gal emission merges in region affected by rfi: parms uncertain

1-513: no identifiable opt counterpart, extended HI: part of HVC complex

1-524: gal emission merges in region affected by rfi: parms uncertain

1-531: on edge of region affected by rfi; id with very faint, lsb object is tentative; caveat emptor

1-532: gal emission merges in region affected by rfi: parms uncertain

1-534: on edge of band, ragged data

1-538: gal emission merges in region affected by rfi: parms uncertain

1-541: gal emission merges in region affected by rfi: parms uncertain

1-543: gal emission merges in region affected by rfi: parms very uncertain

1-556: no identifiable opt counterpart: compact HVC

1-563: gal emission merges in region affected by rfi, but params only mildly affected

1-578: no unambiguous opt counterpart; blue obj in vicinity; marginal detection

1-611: N5221, highly disturbed

1-613: optical identification assigned to blue obj superposed onto E galaxy at similar cz: merger underway? N5221 is $6'$ N, highly disturbed

1-621: on edge of band, ragged data

1-636: ambiguous opt id: possible opt counterpart are 134124.7+151630 and 134119.4+151553

1-639: HI source may be extended to NW and SE of center

1-645: ambiguous opt id; 134233.9+130210 is alternative candidate, $20''$ farther from HI center

1-665: marginal det; tight pair; other possible opt counterpart at 134739.2+154404

1-667: blend; optical counterpart is interacting pair VII Zw 338

1-673: ambiguous opt id; 134941.6+155702 is alternative candidate

1-692: extended HI, no opt counterpart: IVC

1-700: HI emission merges in rfi; params. highly uncertain; opt gal in pair, alternative possible opt. counterpart at 135452.3+140741

1-710: emission blended with 233714, parms uncertain

1-711: see 230859

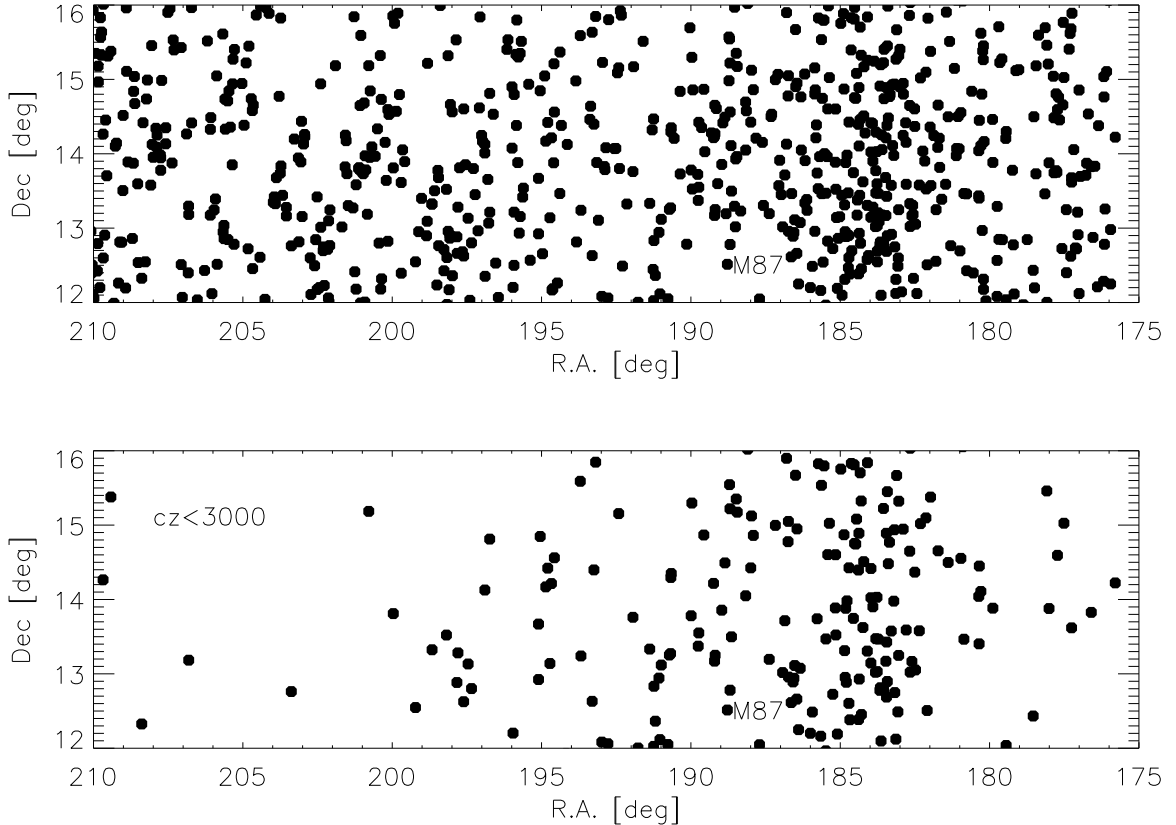1-722: blend with emission by several other objects within $1.5'$

Fig. 2.— Sky distribution of HI candidate detections listed in Table 1: all objects in upper panel, objects with $cz < 3000$ km s^{-1} in the lower one. A label identifies the position of M87, in the vicinity of which HI sources cannot be effectively surveyed because of standing waves and large increase in system temperature contributed by its strong continuum emission; see Section 2.2.

4. Statistical Properties of the ALFALFA HI Sample

The distribution by detection code of HI detections listed in Table 1 is as follows: 24 (4%) are HVCs, 120 (16%) are of type "2", i.e. "priors" of low S/N but corroborated by optical redshifts, and 586 ($\sim$80%) are detections of type "1", of quality fair to excellent.

The 132 deg^2 region of the sky covered by the sample of HI detections listed in Table 1 has been intensely investigated by a variety of studies, including surveys of the Virgo cluster and the SDSS. Targeted observations of optically selected samples amounting to many hundreds of hours of telescope time have yielded detections for 158 objects in the *GOLDMINE* compilation of Gavazzi *et al.* (2003), some of which are fainter than the ALFALFA detection limit (and required a lot more integration time). The blind HI Virgo HIJASS survey (Davies *et al.* 2004) is partly contained within the survey area presented here. In the HIJASS region of full sensitivity which overlaps our ALFALFA dataset, HIJASS found 15 HI detections; in contrast, we detect 193 HI sources in the same region. We detect both the HI plume found near NGC 4388 (Oosterloo & van Gorkom 2005) referred to as Virgo HI4 by Davies *et al.* 2004 and the extended emission

in the vicinity of the "dark galaxy" Virgo HI21 (Davies *et al.* 2004; Minchin *et al.* 2005) showing a clear connection to NGC 4254; we will discuss this structure elsewhere (Haynes *et al.* in preparation). Likewise, the improvement over HIPASS is impressive. In the region containing the 730 HI detections included in Table 1, the HIPASS dataset includes only 40 objects (Wong *et al.* 2006). Of those, several show large position offsets with respect to multiple ALFALFA detections lying within a single Parkes beam, and two are not confirmed by ALFALFA.

The median distance of this sample is 102 Mpc. As of late August 2006, 72% of the ALFALFA HI detections presented here have optical or HI redshifts previously known and 28% are new. The percentage of ALFALFA sources which are new HI detections is 69%. In view of the fact that numerous HI studies have been conducted in this region, largely based on optically selected targets, the percentage of 69% *new* HI detections illustrates the fact that previous HI surveys, generally based on flux– or size–limited, optically selected samples, missed the majority of HI sources: the conventional wisdom on which optical targets would turn out to be HI–rich appears to have been limited.

About 25% of ALFALFA detections have $cz < 3000$ km s^{-1} . The fraction of local objects in the catalog presented here is enhanced by the fact that the region sampled crosses the supergalactic plane and the northern part of the Virgo cluster, one of the densest regions of the Local Supercluster. The detection rate, of about 5.4 objects (4.4 of detection code 1) per square degree, is thus enhanced by a circumstance associated with the characteristics of the large–scale structure of the galaxy distribution in the local Universe. Were it not for the enhancement in the detections within the Local Supercluster, the detection rate would have been lower by about one fifth. This can be visually gauged by inspection of Figure 2, which shows the sky distribution of all the detected sources in the upper panel and that of objects with $cz < 3000$ km s^{-1} in the lower panel.

As mentioned in Section 2.2, the region of about 1° to 1.5° radius about the location of M87 is contaminated by the high brightness of its strong radio source which not only increases the system temperature but also induces strong standing waves. Therefore, the sky region around M87 cannot be sampled by HI spectroscopy, except for the very brightest HI sources. The location of M87 is indicated in Figure 2, at the center of a region of rarefied density of HI detections.

The upper panel of Figure 3 shows the redshift distribution of the galaxies in the current sample. The signatures of the Virgo cluster at the low velocity end and of other features in the large–scale structure of the local Universe are clearly evident. The lack of detections on a strip nearly 1000 km s^{-1} wide near $cz \simeq 15000$ km s^{-1} reflects a bias of the survey. It corresponds to a spectral region heavily and nearly continuously affected by rfi, as shown in Figure 1. The lower panel of Figure 3 shows the analogous diagram for the galaxies with known optical redshifts in the same region of the sky. The large-scale distribution properties of both samples are very similar. The most notable difference between the two plots is the rarefaction of sources at higher cz in the HI panel.

Figure 4 summarizes the distribution in the values of heliocentric velocity $cz_\odot$, velocity width $W50$, flux integral F_c, signal–to–noise ratio S/N and HI mass M_{HI} for the candidate HI detections reported in this catalog. We remind the reader that this survey is not designed to be complete to a given flux integral limit, but rather that the sensitivity limit is a function of velocity width, as discussed in Paper I, Paper II and further below. We also note the paucity of sources with reported HI mass below 10^7 $M_\odot$ in Figure 4(e); while this may be due to a truly low cosmological population of low mass HI sources, the effect is likely to be, at least in part, spurious. As distances have been inferred from redshifts alone, albeit with the aid of a peculiar velocity flow model, the model yields highly uncertain distances within the region sampled, due

to the presence of the Virgo cluster: a very nearby, low velocity object is far more likely to be assigned the Virgo cluster distance by the flow model than a Virgo cluster object of low velocity to be assigned a low distance. The presence of the Virgo cluster may thus operationally "displace" nearby objects, if any, making them appear farther than they truly are. Figure 4(e) suggests that such may indeed be the case, as the number of objects plotted between $10^{7.5}$ and 10^8 $M_\odot$ is overabundant for any reasonable shape of the HI mass function, in comparison with the higher mass bins. Redshift–independent distance estimates of those objects are necessary, if a reliable determination of the HI mass function in Virgo and in the field is to be obtained. This issue will be addressed in a forthcoming paper by Kent et $al.$ (2007, in preparation).

Figure 5(a) displays a plot of HI mass versus distance for all objects in Table 1. Vertical dotted lines outline the distance interval within which our survey is unable to detect any cosmic sources, due to the intrusion of rfi. Galaxies in the Virgo cluster appear as the vertical feature near $D = 17$ Mpc. Figure 5(b) shows that the S/N limit of the survey is relatively independent of velocity width. Sources with velocity widths larger than a few hundred km s^{-1} are apparently identified reliably by our signal extraction algorithm. Very few objects are found with velocity width smaller than 25 km s^{-1} . Several candidate detections are obtained with narrow widths; they lie generally near the detection limit and have no identifiable optical counterparts. Most of them are believed to be due to rfi. Determination of their nature will require follow–up corroborating observations.

Figure 5(c) shows the dependence of the survey's limiting flux integral on velocity width. The dotted line indicates a detection threshold of $S/N = 6.5$, assuming that a spectral smoothing width of $W50/20$ can be adopted for features as wide as 400 km s^{-1} , and a constant value of $400/20$ for features wider than 400 km s^{-1} (see description of Col. 8 of Table 1). The fact that the lower envelope of the data points appears consistent with a slope of $1/2$, rather than steepening to a slope of 1, indicates that our adoption of a smoothing width is essentially correct.

5.   Positional Accuracy of HI Sources

The main purpose of this work is to make available to the general community a data set of HI detections, with analysis of the overall properties of the sample kept at a minimum in the interest of speedy delivery. We address the reader to Paper I and Paper II, in which a preliminary analysis was discussed. However, because of the dependence of the performance properties of the Arecibo telescope on the direction in which it points, some characteristics of the ALFALFA samples will be sky zone dependent. One of such characteristics is the positional accuracy of the HI detections, which carry the imprint of the telescope pointing errors. Thus we devote this section to a brief analysis of that matter. The corrections we will find are specific to the data set presented here.

Positional accuracy of HI sources is of paramount importance per se and in making identification with sources from other catalogs. The main limiting factor for ALFALFA sources is of course the resolution of the ALFA beam. As discussed in Paper I, the ALFA beams are slightly elliptical, with half-power-full-widths of $3.3'$ and $3.8'$. The major axis of the beam is always directed along the position of the telescope's azimuth arm; the vast majority of the ALFALFA observations and all those presented in this paper are made with the azimuth arm in the North-South direction, thus the beam's major axis is in the Declination direction.

ALFALFA samples the sky every second in R.A. and every arcminute in Dec. However, sources are extracted — and their positions measured — after the data are converted to a spatial grid sampled at $1' \times 1'$. A Gaussian weight function is applied as part of the regridding process, which reduces the spatial

resolution of the data to $3.8' \times 4.3'$. An automatic source extraction algorithm identifies a source candidate, which is successively measured and "extracted" interactively by an observer. The spectral extent of the feature is gauged and a 2–D map of the emission is integrated over that full spectral extent. Ellipses are fitted to the image at a set of fixed isophotal levels as well as at the half–power and quarter–power of the peak level, as measured in flux density units per beam area. The position of the source is assumed, in all cases, to be the center of the half-power ellipse. This has proved to be the best choice for the vast majority of sources, as they are generally unresolved by the ALFA beam. Caution is necessary when sources are extended and do not display a clear center of symmetry. A more detailed description of the positional parameter estimates will be presented elsewhere, together with the overall description of the ALFALFA data processing pipeline (Giovanelli *et al.* 2007, in preparation).

The second most important parameter regulating the quality of the ALFALFA positions is the S/N of the HI emission. High S/N sources allow more accurate centroiding than low S/N ones, as discussed below.

The third important influence on ALFALFA positions is the quality of the Arecibo telescope pointing. The telescope can set with a repeatable accuracy of a few arcsec; however, the pointing algorithms which use fits to the telescope configurational parameters yield systematic pointing errors which may, at L band, add up to $15''$ or more. The highest pointing errors occur at the lowest zenith angles. The chosen observing mode for ALFALFA, which freezes the telescope configuration at fixed azimuth, largely allows recovery and correction of the systematic pointing errors.

Positional accuracy is discussed here by using the positional differences between the HI emission ellipse centers and the centers of the galaxies which are identified as optical counterparts. Those differences will include systematic telescope pointing offsets, occasional mismatch in the extent and center of optical and HI source, statistical errors in the HI centroiding and misidentification of optical counterparts. Errors in the centroiding of the optical sources are negligible in comparison. A similar exercise to the one described below has been carried out by comparing ALFALFA positions of continuum radio sources with interferometic positions. Those results are in agreement with those discussed here and will be presented elsewhere (Kent et al. 2007, in preparation).

Figure 6 shows the positional differences (HI minus optical), respectively in R.A. (Δra) and in Dec. (Δdec), expressed in arcsec. The data are split into four panels differing in Declination range, within bins of $1°$. The frame labeled "Dec 12" refers to sources between Dec $= +12°$ and Dec $= +13°$ and so on. As the observations were made with the telescope's azimuth arm oriented N–S, a degree of Declination converts exactly in 1 degree of zenith angle; the latitude of the Arecibo telescope is $+18° \ 20' \ 37''$ N. The plot includes all the sources presented in Table 1, for which an optical identification was made. The HI positions used are those obtained *before* any correction for telescope pointing errors was applied. These sources were all observed at the same azimuth of $0°$ and zenith angles between $2.3°$ and $6.4°$. A systematic offset in the center of the distribution towards positive Δra and negative Δdec is apparent in all panels, with that offset becoming progressively larger with increasing Declination, i.e. decreasing zenith angle. This offset mimics the telescope pointing errors (see "pointing errors" at the website *http://www.naic.edu/∼phil/sysperf/sysperf.html#alfa*) which increase as the telescope points closer to the site's zenith. The amplitude of the pointing errors is indicated by the insets in each plot, expressed respectively by the mean and the median.

Figure 7 shows the distribution of positional offset between HI and optical positions after the systematic pointing errors described above have been removed from the HI positions. The separation of the data into four panels in this case is by S/N. The systematic pointing error that was removed is a simple function of Dec., i.e. zenith angle, obtained for each source by interpolating between the offsets shown in Figure 6.

The HI source positions corrected for this systematic error are those listed in column 2 of Table 1. The dispersion of the positional differences about the center is, as expected, dependent on S/N. For the higher S/N objects ($S/N > 12$), ALFALFA positions are on average accurate to about 15″. ALFALFA positions are significantly better than those obtained with the precursor run reported by Paper II (median difference between HI and optical position of 34″). This is due to two reasons: (i) the ALFALFA data include two full sweeps of each region of the sky with ALFA, hence yielding twice as dense a spatial sampling in Dec. as most of the data in the precursor run; (b) the technique used to extract positional information, which fits ellipses to isophotal contours, is more accurate than that used for the precursor run data.

6.   New Discoveries, Future Work and Conclusions

The principal aim of ALFALFA is to obtain an accurate census of HI-bearing objects in the local universe. The catalog of candidate HI detections presented in Table 1 yields a first picture of the "ALFALFA sky". As discussed in Section 4 and shown in Figure 4, ALFALFA detections span five orders of magnitude in HI mass, and include both massive spirals out to $z \sim 0.06$ and dwarf galaxies within a few Mpc of the Milky Way. The region sampled by the present paper is strongly affected by local large scale structure (the Virgo Cluster), as evident in the redshift distribution presented in Figures 4 and 3. Detailed studies regarding environmental influences on HI content, the HIMF and other characteristics will be incrementally enabled as further installments of ALFALFA data become available.

The principal conclusions which can be gleaned from this first installment of ALFALFA sources in a region covering 132 deg^2, which represents only 1.9% of the final survey, are:

- The ALFALFA survey is delivering high quality 1.4 GHz spectral line data as anticipated. The adopted "minimum intrusion" observing technique (Paper I) is highly successful at reducing spectral baseline instability, beam and sidelobe variations and gain instabilities. Through a combination of deliberate calibration technique and empirical checks, the positional and photometric accuracy of extracted sources is meeting or even exceeding anticipated survey design specifications.

- Although this region of the sky has been previously targeted heavily by surveys of optically selected galaxies (Gavazzi *et al.* 2003) and was covered by both the HIPASS (Wong *et al.* 2006) and HIJASS (Davies *et al.* 2004) Virgo cluster surveys, 69% of the HI detections presented here are new. The improvement over HIPASS in this region is a factor of 18 in the number density of HI detections. The galaxies detected by ALFALFA include a population of gas-rich, star-forming low surface brightness galaxies which are not included in previous optical magnitude-limited surveys.

- The median redshift of ALFALFA in this region of the sky is ~ 7000 km s^{-1} , This depth may be compared to that of HIPASS: ~ 2800 km s^{-1} (Meyer *et al.* 2004). ALFALFA samples volumes well beyond the Local Supercluster, and the distribution of HI detections follows the large scale structure evident in the region. Eventually, we will use the ALFALFA dataset to measure cosmological parameters such as the clustering properties of the HI population and its bias parameter, and to explore further the "void problem" (Peebles 2001).

- 27 of the HI sources are identified with galaxies of early morphology, types E, dE/Sph or S0. Half are in the vicinity of the Virgo cluster and could be members. A study of the characteristics of these objects and the morphology and kinematics of the HI is under way by Koopmann *et al.* (2007, in preparation).

- Among the objects tabulated as HI detections here, several appear to be extended complexes of HI clouds. Referring to them by their AGC number (cat. nr.), 226054 (1-235), 226055 (1-238), 226056 (1-239) and 224316 (1-241) are different clumps of the "dark galaxy" Virgo HI21 reported by Davies *et al.* (2004). The ALFALFA observations show that this feature is clearly connected to the nearby one-armed spiral NGC 4254; we discuss these observations in more detail elsewhere (Haynes *et al.* 2007, in preparation).

- For 41 HI sources, we have been unable to identify unambiguously their optical counterparts. More than half of these are found at redshifts less than $+200$ km s^{-1} and are likely to be perigalactic HVCs. Particularly notable among them are the compact HVCs with positive velocities, a peculiar population in the vicinity of the North Galactic pole. A number of the objects reported by de Heij, Braun & Burton (2002) with fluxes close to the detection limit of that survey are not confirmed by the more sensitive ALFALFA observations (Kent *et al.* 2007, in preparation). The objects with positive velocity which are confirmed, and a few previously undetected with similar velocities, lie in the same sky region as several distant perigalactic structures exhibiting positive velocities: the Bootes dwarf spheroidal galaxy (Belokurov *et al.* 2006a; Muñoz *et al.* 2006), the leading arm of the Sagittarius stream and others found in the the "Field of Streams" (Belokurov *et al.* 2006b), and farther away but still at ~ 200 km s^{-1}, the Local Group galaxy GR 8. We are in the process of investigating the interpretation of these features in more detail.

- For some of the remaining objects without clear optical identifications, possible optical counterparts exist, but the positional accuracy of the ALFALFA HI data is insufficient to yield an unambiguous identification. Interestingly, 17 of the candidate HI detections with no discernible optical counterpart are unlikely to be HVCs. In the case of 215217 (1-62), 226061 (1-257), 226080 (1-316) and 223449 (1-271), galaxies are seen within few arcminutes of the HI positions, which have redshifts comparable with those of the HI features. AGC 226080 has been shown by Oosterloo & van Gorkom (2005) to be a plume extending from NGC 4388. AGC 223449 may have very low HI mass, although its distance is highly uncertain. It remains to be verified whether a connection between the optical and HI objects exists. In the case of 225998 (1-173), another object of highly uncertain distance, a HI–rich galaxy (U7235=NGC4189, 1-175) is found at comparable redshift, but half a degree away. AGC 226118 (1-354) could be an interesting feature in the Virgo cluster, but its vicinity to M87 makes the detection doubtful in spite of a better than fair S/N. AGC 215230 (1-44), 226043 (1-185), 226117 (1-352), 226119 (1-360) nd 226120 (1-366) have velocities in excess of 4000 km s^{-1} ; most in that group are marginal candidate detections. All others sources have identified optical counterparts, thanks to the good positional accuracy of ALFALFA source candidates. A preliminary analysis of Virgo cluster HI sources with no optical counterparts is given in Kent *et al.* (2007, in preparation).

In summary, we present the first catalog release of the ALFALFA survey, corresponding to 1.9% of the projected sky coverage of the completed survey. As anticipated, ALFALFA delivers a dramatic improvement in HI detection sensitivity over previous HI blind surveys through its combination of wide areal coverage, smaller beam area, higher spectral resolution and the sheer sensitivity superiority offered by Arecibo's huge collecting area. The vast majority of HI sources listed in the present catalog have identified optical counterparts. Many are vigorously star-forming yet optically faint, late-type galaxies. Among those HI sources which cannot be unambiguously identified with an optical galaxy, we find a population of HVCs, including ones at significant positive velocity, and a few legitimately extragalactic objects whose optical counterparts are not yet identified.

In addition, the survey identifies nearly as many candidate detections of lower S/N, including many with narrow spectral lines and no optical counterparts. Because candidate source reliability plummets below S/N < 5, these HI candidates are not reported here but are targeted for corroborating follow–up observations with the Arecibo L-band wide system employing an efficient strategy designed for that purpose, as discussed in Paper I.

A catalog of comparable size, covering a strip of the same R.A. extent and including the southern part of the Virgo cluster, is in preparation (Kent *et al.* 2007, in preparation); eventually, ALFALFA will cover the entire region included in the Virgo Cluster Catalog (Binggeli, Sandage & Tammann 1985). Catalog data releases for other parts of the sky are also in preparation by several groups within our collaboration, as are programs involving multiwavelength follow–up studies of selected targets presented here.

The catalog presented here and its associated data products will be incorporated into the more extensive digital HI dataset at *http://arecibo.tc.cornell.edu/hiarchive* as part of the ALFALFA Arecibo legacy.

REFERENCES

Barnes, D.G, Staveley–Smith, L., de Block, W.J.G., Oosterloo, T. Stewart, I.M. *et al.* 2001, MNRAS, 322, 486

Belokurov, V., Evans, N.W., Irwin, M.J., Hewett, P.C., & Wilkinson, M.I. 2006a, ApJ, 637, L29

Belokurov, V., Zucker, D. B., Evans, N. W., Gilmore, G., Vidrih, S., *et al.* 2006b, ApJ, 642, L137

Binggeli, B., Sandage, A. & Tammann, G.A. 1985, AJ, 90, 1681

Chamaraux, P., Balkowski, C. & Gerard, E. 1980, A&A 83, 38

Dale, D.A. & Giovanelli, R. 2000, ASP Conference Series Vol. 201, ed. by S. Courteau & J. Willick, p. 25

Davies, R.D. & Lewis, B.M. 1973, MNRAS, 165, 213

Davies, J., Minchin, R., Sabatini, S., van Driel, W., Baes, M. *et al.* 2004, MNRAS, 349, 922

de Heij, V., Braun, R. & Burton, W.B. 2002, A&A, 391, 159

Gavazzi, G., Boselli, A., Donati, A., Franzetti, P. & Scodeggio, M. 2003, A&A, 400, 451

Giovanelli, R. & Haynes, M.P. 1983, AJ, 88, 881

Giovanelli, R., Haynes, M.P., Freudling, W. *et al.* 1998, ApJ, 505, L91

Giovanelli, R., Haynes, M.P., Kent, B.R. *et al.* 2005a, AJ, 130, 2598 (Paper I)

Giovanelli, R., Haynes, M.P., Kent, B.R. *et al.* 2005b, AJ, 130, 2613 (Paper II)

Giovanelli, R. *et al.* 2007, in preparation

Haynes, M.P. *et al.* 2007, in preparation

Kent, B.R. *et al.* 2007, in preparation

Koopmann, R. *et al.* 2007, in preparation

Masters, K.L., Haynes, M.P. & Giovanelli, R., 2004, ApJ, 607, L115

Meyer, M.J., Zwaan, M.A., Webster, R.L. *et al.* 2004, MNRAS, 350, 1195

Minchin, R., Davies, J., Disney, M., Boyce, P., Garcia, D. *et al.* 2005, ApJ, 622, L21

Muñoz, R.R., Carlin, J.L., Frinchaboy, P.M., Nidever, D.L., Majewski, S.R. & Patterson, R.J. 2006, ApJ, 650, L51

Oosterloo, T., & van Gorkom, J., 2005, A&A, 437, L19

Peebles, P.J.E. 2001, ApJ, 557, 495

Rosenberg, J.L. & Schneider, S.E. 2002, ApJ, 567, 247

Saintonge, A. 2007, AJ in press

Shostak, G.S. & Allen, R.J. 1980, A&A, 81, 167

Skrutskie, M.F., Cutri, R.M., Stiening, R., Weinberg, M.D., Schneider, S. *et al.* 2006, AJ, 131, 1163

Solanes, J.-M., Sanchis, T., Salvador–Solé, E. *et al.* 2002, AJ, 124, 2440

Springob, C.M., Haynes, M.P., Giovanelli, R. & Kent, B.R. 2005, ApJS, 160, 149

Springob, C.M., Masters, K.L., Haynes, M.P., Giovanelli, R. & Marinoni, C. 2006, ApJS, (submitted)

Wong, O.I., Ryan–Weber, E.V., Garcia–Appadoo, D.A. *et al.* 2006, MNRAS, 371, 1855

York, D.G., Adelman, J., Anderson, J.E., *et al.* 2000, AJ, 120, 1579

Zwaan, M.A., Meyer, M.J., Staveley–Smith, L. & Webster, R.L. 2005, MNRAS, 359, 30
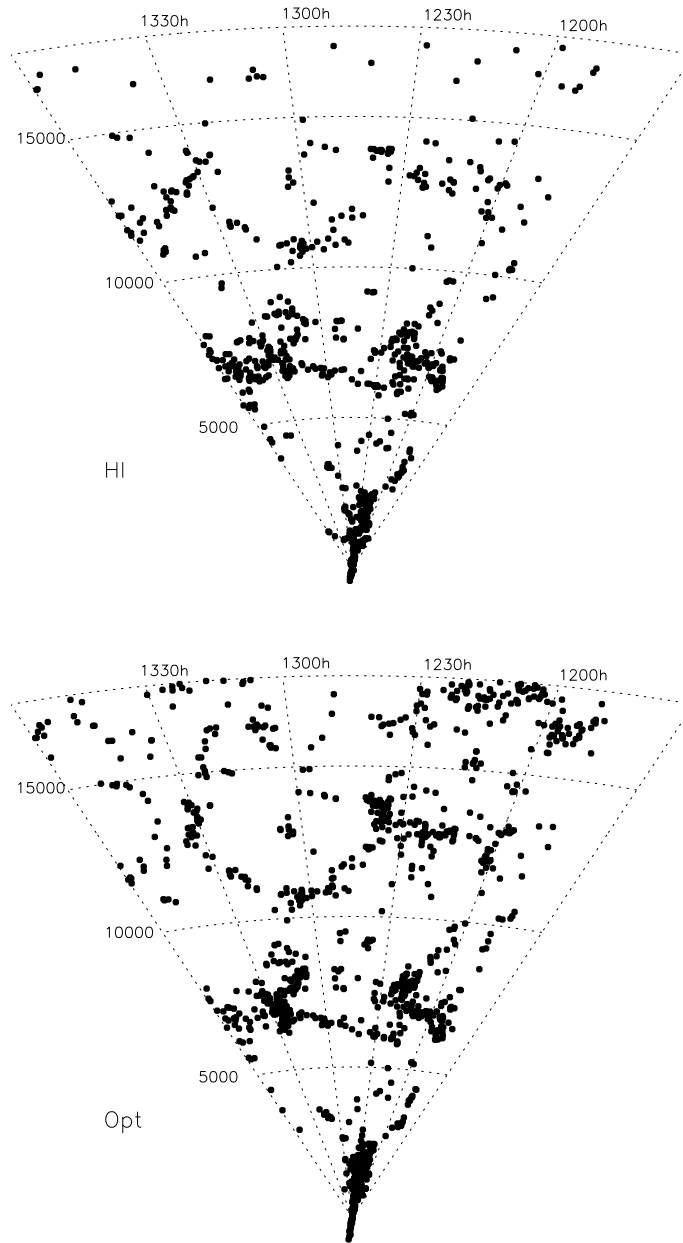
Fig. 3.— Right Ascension vs. recession velocity in km s^{-1} , of all sources listed in Table 1 (upper panel "HI") and analogous plot of galaxies with optical redshifts in the same region of sky (lower panel "Opt"). Note the Virgo cluster in the lower portion of each cone plot.
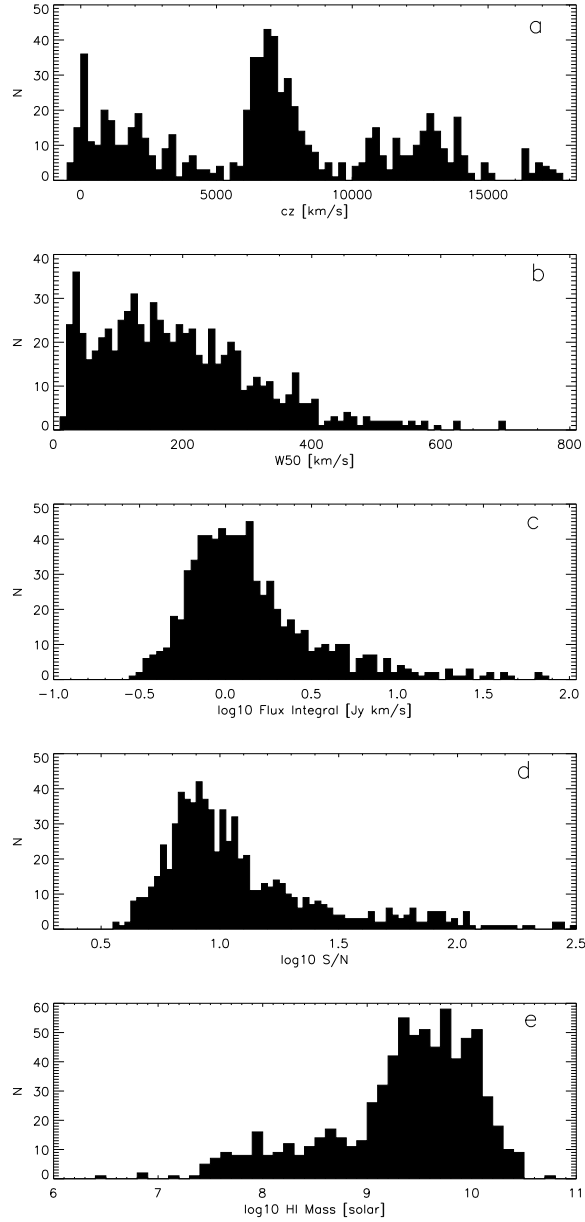
Fig. 4.— Histograms of the HI candidate detections listed in Table 1. From top to bottom: (a) recessional velocity in km s^{-1} ; (b) HI line width W$_{50}$ in km s^{-1} ; (c) log base 10 of the flux integral in Jy km s^{-1} ; (d) the peak signal-to-noise ratio, in logarithmic units; (e) the derived HI mass, in logarithmic units of $M_\odot$. Note the "step" in the HI mass histogram near $10^{7.5}$, which is probably an artifact due to uncertainties in galaxy distances in the direction towards the Virgo cluster, as decribed in the text.
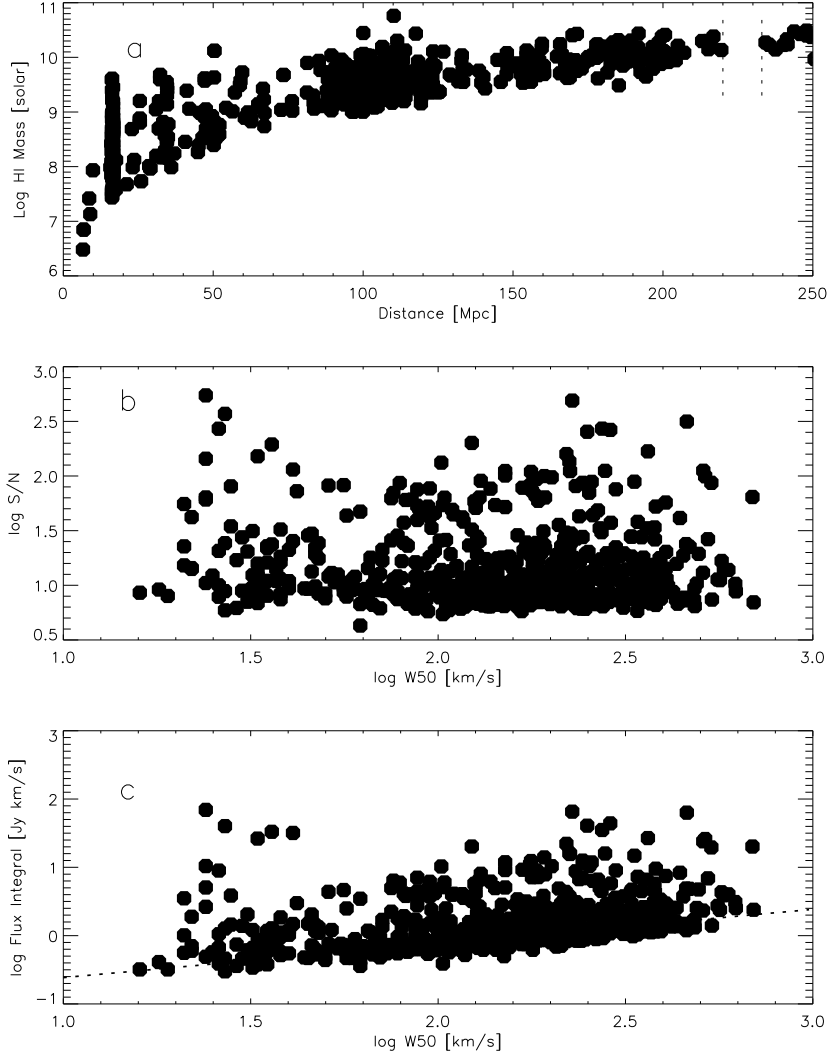
Fig. 5.— (a) HI mass vs. distance for all sources of types 1 and 2 in Table 1. The Virgo cluster is the vertical feature near D=17 Mpc. Cosmic sources within the spectral region between the two vertical dashed lines are inaccessible due to rfi. (b) S/N vs. velocity width for all sources in Table 1. The lower envelope appears to be independent of S/N, indicating that no significant bias is present in the detection of sources of large width. (c) Flux integral vs. velocity width. The dashed line corresponds to a S/N limit of 6.5.
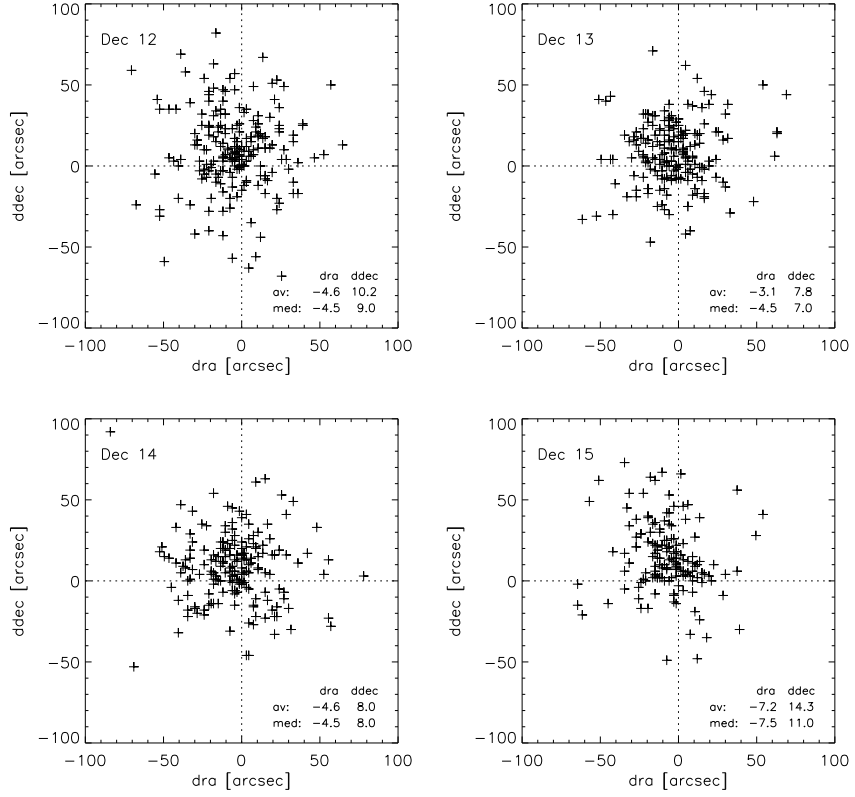
Fig. 6.— Differences between the positions of the HI sources, *before applying a correction for telescope pointing errors*, and the optical counterpart positions as listed in Col. 4 of Table 1. Sources are separated by Declination bins of 1°: the label "Dec 12" identifies sources with Declination between +12° and +13°, etc. Average and median offsets, expressed in arcsec, are inset within each panel.
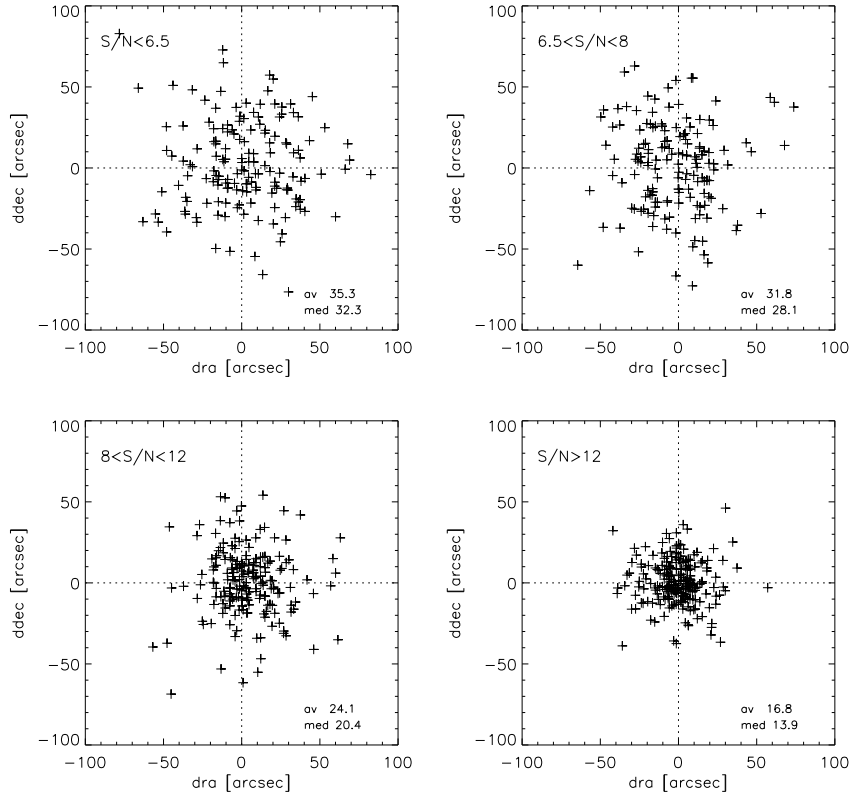
Fig. 7.— Differences between the positions of the HI sources, as indicated by the values in Col. 3 of Table 1, which are corrected for systematic telescope pointing errors, and the optical counterpart positions as listed in Col. 4 of Table 1. Sources are separated by S/N as indicated in each panel. Average and median offsets, expressed in arcsec, are inset within each panel.